Hierarchical Multiscale Simulation of Electrokinetic Transport in Silica Nanochannels at the Point of Zero Charge

Sony Joseph and N. R. Aluru*

Department of Mechanical Science and Engineering, Beckman Institute for Advanced Science and Technology, University of Illinois at Urbana−Champaign, Urbana, Illinois 61801

Effects of nanoscale confinement and partial charges that stem from quantum calculations are investigated in silica slit channels filled with 1 M KCl at the point of zero charge by using a hierarchical multiscale simulation methodology. Partial charges of both bulk and surface atoms from ab initio quantum calculations that take into account bond polarization and electronegativity are used in molecular dynamics (MD) simulations to obtain ion and water concentration profiles for channel widths of 1.1, 2.1, 2.75, and 4.1 nm. The interfacial electron density profiles of simulations matched well with that of recent X-ray reflectivity experiments. By simulating corresponding channels with no partial charges, it was observed that the partial charges affect the concentration profiles and transport properties such as diffusion coefficients and mobilities up to a distance of about 3 σ_{O-O} from the surface. Both in uncharged and partially charged cases, oscillations in concentration profiles of K^+ and Cl^- ions give rise to an electro-osmotic flow in the presence of an external electric field, indicating the presence of an electric double layer at net zero surface charge, contrary to the expectations from classical continuum theory. $I-V$ curves in a channel-bath system using ionic mobilities from MD simulations were significantly different for channels with and without partial charges for channel widths less than 4.1 nm.

I. Introduction

Transport and electrochemical phenomena in synthetic nanochannels is of growing interest in biomimetic nanoscale devices. Recent advances in the fabrication of "lab-on-a-chip" ultraconfined fluidic systems[1] and synthetic nanopores[2,3] raise fundamental questions about the influence of surfaces on ion transport. The surface charge induced electrostatic ion (Debye) screening and electrokinetic effects such as electro-osmosis can have large effects on the conductance in nanochannels.[4−6] Electrolyte−oxide interfaces play a key role in detection, precipitation, or adsorption of toxic agents. The silica−electrolyte interfacial dynamics and the effects of nanoscale confinement on the transport properties of ions and water need to be resolved for characterization and design of silica nanochannel-based devices and sensors.

The interactions between water and the oxide surface of minerals have been studied by models of the electric double layer.[7] Despite the widespread application of such surface complexation models, much uncertainty surrounds the choice of values of the parameters for the models which depend on the specific oxide and type of electrolyte and yet often they cannot be directly measured.[7] In continuum theories,[8] electrostatic interactions are treated with the Poisson−Boltzmann (PB) mean-field approximation. It has been shown that the PB approximation can be inaccurate, as it cannot capture the finite ion size effects and the hydration forces which arise due to the specific structure of water.[9] In mean-field theories such as the Poisson−Nernst−Planck (PNP) and PB, walls are assumed to have a smeared out uniform surface charge. The validity of this approximation has been questioned in nanoscale systems where modified mean-field theories,[10,11] Monte Carlo simulations,[12] and atomic scale simulations[9] have shown that the discrete nature of the surface charge alters the ion distribution near the surface. In relatively nonpolar walls, the local charge variations on the wall have a relatively minor role, but in highly polar surfaces such as quartz, the localized charge density due to bond polarization and electronegativity is of primary importance when dealing with wall−fluid interactions. In addition to classical Coulombic interactions, quantum effects such as exchange−correlation also play a role in the molecular electrostatic potential generated by the wall. Extremely small orders of time and length scales are possible in a full scale ab initio molecular dynamics (MD), and this makes it unsuitable for investigating macroscopic electrokinetic transport in nanochannels.

In this paper, we employ a hierarchical multiscale approach for a full-scale characterization of water and ion transport in nanochannels. First, using the density functional theory(DFT), the molecular electrostatic potential which accounts for the quantum effects at the silanol surface is calculated. Partial atomic charges on the wall atoms are computed using a molecular electrostatic potential fit which are then used as inputs for MD. Transport coefficients such as mobilities and diffusion coefficients are then computed from MD simulations. Finally, the transport coefficients are used in the PNP equations to calculate the experimentally observable current−voltage characteristics.

The surface chemistry and interfacial properties of silica−water/electrolyte interface can be quite complex.[13] Silica can occur in amorphous or crystalline forms and can be hydroxylated

* To whom correspondence should be addressed. E-mail: aluru@uiuc.edu. URL: https://www.uiuc.edu/~aluru.

(1) Kerby, M.; Spaid, M.; Wu, S.; Parce, J.; Chien, R.-L. *Anal. Chem.* **2002,** *74,* 5175.
(2) Kuo, T.-C.; Sloan, L.; Sweedler, J.; Bohn, P. *Langmuir* **2001,** *17,* 6298.
(3) Ho, C.; Qiao, R.; Heng, J. B.; Chatterjee, A.; Timp, R. J.; Aluru, N. R.; Timp, G. *Proc. Natl. Acad. Sci. U.S.A.* **2005,** *102,* 10445.
(4) Stein, D.; Kruithof, M.; Dekker: C. *Phys. Rev. Lett.* **2004,** *93,* 035901.
(5) Schoch, R. B.; Renaud, P. *Appl. Phys. Lett.* **2005,** *86,* 253111.
(6) Qiao, R.; Aluru, N. R. *Phys. Rev. Lett.* **2004,** *92,* 198301.
(7) Sverjensky, D. A. *Geochim. Cosmochim. Acta* **2001,** *65,* 3643.
(8) Lyklema, J. *Fundamentals of Interface and Colloid Science*; Academic: San Diego, 1995.

(9) Qiao, R.; Aluru, N. R. *J. Chem. Phys.* **2003,** *118,* 4692.
(10) Moreira, A. G.; Netz, R. R. *Europhys. Lett.* **2002,** *57,* 911.
(11) Lukatsky, D. B.; Safran, S. A.; Lau, A. W. C.; Pincus, P. *Europhys. Lett.* **2002,** *58,* 785.
(12) Khan, M. O.; Petris, S.; Chan, D. Y. C. *J. Chem. Phys.* **2005,** *122,* 104705.
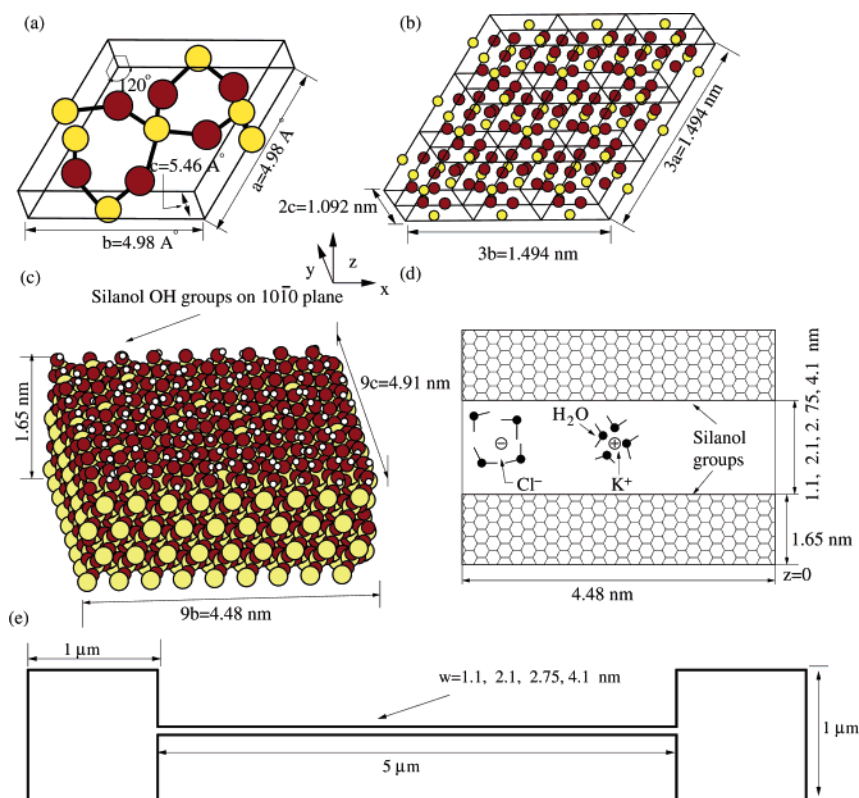(13) Iler, R. K. *Chemistry of Silica*; John Wiley and Sons: New York, 1979.

Figure 1. Simulation system setup. (a) Quartz unit cell. Circles with the darker shade represent oxygen atoms, and the circles with the lighter shade represent silicon atoms. The unit cell has three Si and six O atoms. In the figure, silicon atoms at the unit cell edges and surfaces have also been included. (b) The DFT simulation domain comprising of $3 \times 3 \times 2$ unit cells. (c) Channel wall for MD simulations made by periodic replication of the unit cells. In the x and y directions, nine cells were replicated. In the z direction, a transformation was made from the parallelepiped to the rectangular structure. Silanol terminations on the surface after removing a layer of surface silicon atoms is also shown. (d) Schematic of the MD simulation. The axial length is 4.48 nm, and the width of each channel wall is 1.65 nm. (e) The continuum simulation domain.

with silanol end groups or dehydroxylated. Irrespective of the differences in their origin, it is the concentration and distribution of surface hydroxyl groups and the pH of the solution that control the chemistry of a silica surface and hence properties such as adhesion and adsorption. Since water physisorption mainly happens on surface silanol groups, it seems reasonable to separate the process of chemisorption (hydroxylation of surface sites) and water physisorption. Instead of simulating the whole reaction process, we consider a neutral, fully hydroxylated crystalline α-quartz surface at the pristine point of zero charge formed by adsorption of water on a cleaved or non-hydroxylated surface forming silanol groups on the interface. There is no further dissociation of the silanol groups, and the net charge of the surface is zero. The point of zero charge is of particular interest in interfacial electrokinetics of oxides in determining the net surface charge at various pH values. In this study, we limit ourselves to the interfacial phenomena at the point of zero charge. Even though the surface may not have any net charge, localized electron density distribution due to the difference in electron affinity of silicon and oxygen and the effects of bond polarization can be represented by partial charges on the atoms. Although typically micro/nanofluidics systems use amorphous silica surfaces to isolate the effects due to the partial charges from that due to structural inhomogeneities arising from defects and dangling bonds, we use crystalline α-quartz surfaces, where experimental interfacial electron density is available in the literature.

The hypothesis of the existence of an electric double layer at zero surface charge has been confirmed recently by Dukhin et al.[14] based on their experimental measurements of ζ potentials at zero surface charge for alumina−KCl interfaces. Mancui and

Ruckenstein[15] had investigated this phenomena using a modified PB theory and suggested mechanisms such as van der Waals interaction between ions and the media, ion size effects, and changes in dielectric constant. However, questions such as the role of water, the effect of the localized charge distribution of the wall on the double layer, etc. have still not been addressed adequately. Moreover, since MD includes explicit water molecules, a better understanding of the underlying mechanisms can be obtained using MD simulations.

To understand the electrokinetic transport in channels with a net zero surface charge and to characterize the quantum-mechanical effects, we investigate transport in two types of channels (i) with wall partial charges from quantum calculations and (ii) without any partial charges. We report electrokinetic transport in α-quartz channels of four different widths (4.1, 2.75, 2.1, and 1.1 nm) with 1 M KCl. Figure 1 shows the three levels of simulation hierarchy and the construction of the channel. In the following sections, we discuss in detail the multiscale framework used. We first describe the calculation of partial charges and compare them with existing calculations and experiments. After matching the MD simulations performed with these partial charges with experimental electron density observations, we calculate the transport properties as a function of the channel width. Finally, the transport properties from MD simulations are used to compute macroscopic $I-V$ curves in the channels using continuum theory.

(14) Dukhin, A.; Dukhin, S.; Goetz, P. *Langmuir* **2005**, *21*, 9990.
(15) Mancui, M.; Ruckenstein, E. *Adv. Colloid Interface Sci.* **2004**, *112*, 109.

II. Computation of Partial Charges

As far as silica−electrolyte interactions are concerned, among all the interaction parameters in the force field, the partial atomic charges are the most important since (i) they are the only parameters to capture bond polarization arising from quantum effects and (ii) their effects are long range and they can significantly influence the static and dynamic properties of water and ions. When the partial charges are greater than 1.0 e, they cause the Coulombic interaction energy to be greater than that of bond, angle, or torsion energies by approximately 2 orders of magnitude.[16] In force fields commonly cited in the literature, the partial charges of bulk silicon span a wide range from +0.5 e to +4.0 e. Most of the existing calculations were based on geometry-optimized silica clusters consisting of a few atoms rather than on silica slabs. Moreover, in many cases, surface silicon and oxygen atoms have been assumed to have the same charges as bulk atoms. Therefore, we performed density functional quantum calculations using Gaussian03[17] with the B3LYP model[18,19] as the exchange correlation and a 6-31G* split-valence polarization basis set to obtain the partial charges both for the surface and bulk silica and compared them with existing computations and experimental results.

The bulk quartz structure is a trigonal system characterized by 4-fold coordinated silicon atoms and 2-fold coordinated oxygen atoms. The unit cell has three Si and six O atoms, and the primitive vectors are $a = b = 4.98$ Å and $c = 5.46$ Å with $\alpha = \beta = 90°$ and $\gamma = 120°$ (Figure 1a). To form the channel wall surface, the unit cells were periodically replicated along b and c directions with nine unit cells and with four unit cells along the a direction. The surface structure was obtained by removing silicon atoms along the $10\bar{1}0$ plane and attaching hydrogen atoms to the oxygens with a bond length of 1 Å to form a fully coordinated structure with silanol group terminations (Figure 1c).

To obtain the partial charges of the bulk and surface atoms, three types of systems were considered. (i) A quartz unit cell consisting of six oxygen and three silicon atoms which are periodic in all three directions representing bulk silica, (ii) a supercell which is a composite of $3 \times 1 \times 1$ unit cells that is periodic in b and c directions with one unit cell each but with three unit cells in the a direction the oxygens being terminated with silanol groups representing a slab geometry, and (iii) a $3 \times 3 \times 2$ supercell structure (Figure 1b) which is nonperiodic with silanol terminations in all three directions. Both Mulliken[20] partial charges based on partitioning of the electronic charge density within different orbitals and CHelpG partial charges[21,22] obtained by fitting point charges to the molecular electrostatic potential were computed.

(16) Heinz, H.; Suter, U. W. *J. Phys. Chem. B* **2004**, *108*, 18341.

(17) Frisch, M. J.; Trucks, G. W.; Schlegel, H. B.; Scuseria, G. E.; Robb, M. A.; Cheeseman, J. R.; Montgomery, J. A., Jr.; Vreven, T.; Kudin, K. N.; Burant, J. C.; Millam, J. M.; Iyengar, S. S.; Tomasi, J.; Barone, V.; Mennucci, B.; Cossi, M.; Scalmani, G.; Rega, N.; Petersson, G. A.; Nakatsuji, H.; Hada, M.; Ehara, M.; Toyota, K.; Fukuda, R.; Hasegawa, J.; Ishida, M.; Nakajima, T.; Honda, Y.; Kitao, O.; Nakai, H.; Klene, M.; Li, X.; Knox, J. E.; Hratchian, H. P.; Cross, J. B.; Bakken, V.; Adamo, C.; Jaramillo, J.; Gomperts, R.; Stratmann, R. E.; Yazyev, O.; Austin, A. J.; Cammi, R.; Pomelli, C.; Ochterski, J. W.; Ayala, P. Y.; Morokuma, K.; Voth, G. A.; Salvador, P.; Dannenberg, J. J.; Zakrzewski, V. G.; Dapprich, S.; Daniels, A. D.; Strain, M. C.; Farkas, O.; Malick, D. K.; Rabuck, A. D.; Raghavachari, K.; Foresman, J. B.; Ortiz, J. V.; Cui, Q.; Baboul, A. G.; Clifford, S.; Cioslowski, J.; Stefanov, B. B.; Liu, G.; Liashenko, A.; Piskorz, P.; Komaromi, I.; Martin, R. L.; Fox, D. J.; Keith, T.; Al-Laham, M. A.; Peng, C. Y.; Nanayakkara, A.; Challacombe, M.; Gill, P. M. W.; Johnson, B.; Chen, W.; Wong, M. W.; Gonzalez, C.; Pople, J. A. *Gaussian 03*, revision C.02; Gaussian, Inc.: Wallingford, CT, 2004.

(18) Vosko, S. H.; Wilk, L.; Nusair, M. *Can. J. Phys.* **1980**, *58*, 1200.

(19) Lee, C.; Yang, W.; Parr, R. G. *Phys. Rev. B* **1988**, *37*, 785.

(20) Mulliken, R. S. *J. Chem. Phys.* **1955**, *23*, 1833.

(21) Chirlian, L. E.; Francl, M. M. *J. Comput. Chem.* **1987**, *8*, 894.

(22) Francl, M. M.; Carey, C.; Chirlian, L. E.; Gange, D. M. *J. Comput. Chem.* **1996**, *17*, 367.

Table 1. Partial Charge Computations on Different Structures

atom type	1 unit cell	$3 \times 1 \times 1$ supercell	$3 \times 3 \times 2$ supercell	$3 \times 3 \times 2$ supercell
charge type	Mulliken	Mulliken	Mulliken	CHelpG
periodicity	3D	2D	nonperiodic	nonperiodic
bulk Si	1.302	1.302	1.30	1.36
bulk O	−0.651	−0.651	−0.65	−0.68
surface Si	−	1.200	1.197	1.38
surface O	−	−0.625	−0.621	−0.71
silanol O	−	−0.70	−0.69	−0.77
silanol H	−	0.45	0.45	0.44

Table 2. Comparison of Our Bulk Partial Charges with that in Literature

bulk Si (e)	method	ref
+1.36	DFT/B3LYP/6-31G*/CHelpG	this work
+1.30	DFT/B3LYP/6-31G*/Mulliken	this work
+1.2 ± 0.1	experimental (indirect)	23
+1.17	experimental (indirect)	24
+4.0	formal charge	25
+3.3	DFT/Mulliken	26
+2.4	SCF/empirical charge fitting	27,28
+1.8	Pauling (1960)	29
+1.318	charge equilibration	30
+1.0	Pauling (1980)	31
+0.524	SCF/partition/scaling	32
+1.4	MP2/CHelpG	33
+1.346	DFT/Perdew Wang GGA/Mulliken	34
+2.1	DFT/GGA/Mulliken + potential fitting	35
+1.1	semiempirical/extended Born method	16

Table 3. Comparison of Our Silanol Group Partial Charges with that in Literature

hydroxyl O (e)	hydroxyl H (e)	method	ref
−0.95	0.425	DFT/GGA/Mulliken + potential fitting	35
−0.91 to −1.1	0.40	MP2/CHelpG	33
−0.77	0.44	DFT/B3LYP/CHelpG	this work
−0.683	0.36	extended Born method	16
−0.74	0.60	experimental (indirect)	24

Mulliken charges being based on charge partioning correlate well with experimental electron density observations. Since CHelpG charges are based on a molecular electrostatic potential fit, they can capture, though in an approximate way, higher-order effects arising from dipoles and multipoles and are better suited for MD simulations where partial charges are the only parameters used to include the effects of polarization.

Table 1 shows the results from the calculations. It was found that for the $3 \times 3 \times 2$ supercell, the interior atoms had the same Mulliken partial charge as that of a 3D-periodic single unit cell system. Comparisons of the Mulliken charges of the surface atoms on the nonperiodic $3 \times 3 \times 2$ supercell and that of the surface atoms on the nonperiodic surface of the 2D-periodic $3 \times 1 \times 1$ supercell gave very similar values. A nonperiodic supercell, if it is sufficiently large enough, can capture the local electron density distribution as that of a periodic system.

Table 2 is a compilation of partial charges of bulk silicon in the literature with some of the entries from ref 16. Our charges match well with experimental observations. Table 3 contains comparisons for the silanol groups at the surface. In the literature, surface silicon and oxygen atoms in the layer between the bulk and the silanol groups have the same charges as in the bulk, but our charges are shown in Table 1.

III. Molecular Dynamics Simulations

MD simulations were performed with the computed partial charges to obtain the structure and dynamics of water and ions

Table 4. Force Field Parameters Used in Simulation

atom type	σ (nm)	ϵ (kJ/mol)	charge (e)
bulk Si	0.3386	2.4470	1.36
bulk O	0.3169	0.6502	−0.68
surface Si	0.3386	2.4470	1.38
surface O	0.3169	0.6502	−0.71
silanol O	0.3169	0.6502	−0.77
silanol H	0.0	0.0	0.44
water O	0.3169	0.6502	−0.8476
water H	0.0	0.0	0.4238
K^+	0.3331	0.4184	1.0
Cl^-	0.4401	0.4184	−1.0

for various channel widths. The computational domain consisting of the surface atoms and the confined electrolyte is shown in Figure 1d. The structure of each interface was created by periodic replication of the unit cells. The system has two identical $10\bar{1}0$ α-quartz interfaces which are mirror images of each other with respect to the channel center plane. Water and ions are confined in the region between the interfaces. The channel dimensions were $L_x = 9b = 4.48$ nm and $L_y = 9c = 4.91$ nm, and the thickness of the wall is 1.65 nm in the z direction. Periodic replication gives a parallelepiped structure, which was transformed into a rectangular structure with silanol terminations as shown in Figure 1c. Four different channel geometries with separation distance between the walls of 1.1, 2.1, 2.75, and 4.1 nm were considered. The largest distance of 4.1 nm is sufficiently large enough to establish bulk water in the center of the channel.

We consider two types of potentials—Lennard–Jones (LJ) and Coulomb. Table 4 is a summary of the partial charges and the LJ parameters used. The LJ parameters for Si and water were taken from the GROMACS force field,[36] the ions from ref 37, and the ion–Si and O–Si pairs were obtained by using the linear combination rule and the Si–Si parameters from ref 36. The ions are modeled as LJ atoms with point charges. Since the interface is dominated by the silanol groups, the wall-electrolyte van der Waals forces would be dominated by the contribution from oxygen atoms rather than silicon atoms. Most of the past force fields have been primarily developed to characterize the structural properties of silica, and they have complex potentials with many body terms to accurately capture the conformational changes in silica. Since we are primarily interested in the electrokinetic transport and not in the structural properties of silica, flexible bonds are used to model only the surface silanol groups while the interior atoms are held fixed to reduce the computational cost. The flexible bonds in the silanol groups allow for some exchange of momentum and energy of the water and ions with the channel walls. For the silica surface, a $10\bar{1}0$ α-quartz structure

was chosen because recent experimental results in the literature could be used to compare the interfacial water structure.[38]

For water, we used the rigid, nonpolarizable SPC/E model[39] with partial charges for oxygen, $q_O = -0.8476$ e, and two hydrogens, $q_H = +0.4238$, and LJ potential for oxygen with constraints using the SHAKE algorithm. The SPC/E model has been known to reproduce accurately the bulk properties of water especially relevant to electrokinetic transport such as diffusivity and dielectric properties.[40] The number of water molecules is chosen such that the water concentration in the center of the channel is within 1.0% of 55 M. The wall silicon and oxygen atoms were fixed in space. The bonded interactions of the surface silanol groups were modeled using harmonic potentials with the force constants being the same as that in the SPC/E flexible model of water.[36]

The simulation box dimensions along the periodic axes were $L_x = 4.48$ nm and $L_y = 4.91$ nm. Along the nonperiodic z direction, in addition to the wall−electrolyte−wall system, a vacuum of $\approx 2.5-3$ times the width of the wall−electrolyte−wall system was added to obtain $L_z \simeq 15-18$ nm depending on the channel width. Such a vacuum is more than enough for accurate computation of electrostatic interactions using a 2D-periodic PME. A Berendsen[41] thermostat was used to maintain the temperature at 300 K with a time constant of 0.1 ps. The simulation was started from a random initial configuration and equilibrated for 2 ns before taking the statistics. For transport properties such as diffusion and mobility, a simulation time of 7 ns was used for generating enough statistics for calculating the properties as a function of the wall normal distance. For electro-osmotic velocities, 50−70 ns simulation time was required to obtain reliable velocity profiles.

IV. Continuum Calculations

The macroscopic ionic transport in the silica channel is described by the coupled PNP and the Stokes equations[42,43] in continuum simulations which are solved self-consistently to obtain the concentration of the ions, electrical potential, and the bulk velocity. The Poisson, Nernst−Planck, and Stokes equations with the continuity criterion are given below:[44]

$$\nabla^2 \Phi = -\frac{\rho_e}{\epsilon_0 \epsilon_r} \tag{1}$$

$$\Gamma_i = -D_i \nabla c_i - \mu_i z_i F c_i \nabla \Phi + c_i \mathbf{u} \tag{2}$$

$$\nabla \cdot \Gamma_i = 0 \tag{3}$$

$$\mu \nabla^2 \mathbf{u} - \nabla p = \rho_e \nabla \Phi \tag{4}$$

$$\nabla \cdot \mathbf{u} = 0 \tag{5}$$

where Φ is the electrical potential, ρ_e is the charge density in the system, ϵ_0 is the dielectric permittivity in vaccum, ϵ_r is the relative dielectric constant of water, Γ_i is the flux of the species i, z_i is the valence of the ith species, D_i and μ_i are the diffusion

(23) Lewis, J.; Schwarzenbach, D.; Flack, H. D. *Acta Crystallogr., Sect. A* **1982**, *38*, 733.

(24) Belokoneva, E. L.; Gubina, Y. K.; Forsyth, J. B.; Brown, P. J. *J. Phys. Chem. Min.* **2002**, *29*, 430.

(25) Collins, D. R.; Catlow, C. R. A. *Am. Mineral.* **1992**, *77*, 1172.

(26) Terra, J.; Ellis, D. E. *Phys. Rev. B* **1997**, *56*, 1834.

(27) van Beest, B. W. H.; Kramer, G. J.; van Santen, R. A. *Phys. Rev. Lett.* **1990**, *64*, 1955.

(28) Tsuneyuki, S.; Tsukada, M.; Aoki, H.; Matsui, Y. *Phys. Rev. Lett.* **1988**, *61*, 869.

(29) Pauling, L. *The Nature of the Chemical Bond*; Cornell University Press: Itaca, NY, 1960.

(30) Rappe, A. K.; Goddard, W. A. *J. Phys. Chem.* **1991**, *95*, 3358.

(31) Pauling, L. *Am. Mineral.* **1980**, *65*, 321.

(32) Hill, J.-R.; Sauer, J. *J. Phys. Chem.* **1994**, *98*, 1238.

(33) Teppen, B.; Rasmussen, K.; Bertsch, P.; Miller, D.; Schafer, L. *J. Phys. Chem. B* **1997**, *101*, 1579.

(34) van Duin, A.; Strachan, A.; Stewman, S.; Zhang, Q.; Xu, X.; Goddard, W. A. *J. Phys. Chem. A* **2003**, *107*, 3803.

(35) Cygan, R. T.; Liang, J. J.; Kalinichev, A. G. *J. Phys. Chem. B* **2004**, *108*, 1255.

(36) Lindahl, E.; Hess, B.; van der Spoel, D. *J. Mol. Model.* **2001**, *7*, 306.

(37) Koneshan, S.; Rasaiah, J. C.; Lynden-Bell, R. M.; Lee, S. H. *J. Phys. Chem. B* **1998**, *102*, 4193.

(38) Schlegel, M. L.; Nagy, K. L.; Fenter, P.; Sturchio, N. C. *Geochim. Cosmochim. Acta* **2002**, *66*, 3037−3054.

(39) Berendsen, H. J. C.; Grigera, J. R.; Straatsma, T. P. *J. Phys. Chem.* **1987**, *91*, 6269.

(40) Sorenson, J. M.; Hura, G.; Glaeser, R. M.; Head-Gordon, T. *The J. Chem. Phys.* **2000**, *113*, 9149.

(41) Berendsen, H. J. C.; Postma, J. M.; DiNola, A.; Haak, J. R. *J. Chem. Phys.* **1984**, *81*, 3684.

(42) Oldham, K. B.; Myland, J. C. *Fundamentals of Electrochemical Science*; Academic: San Diego, 1994.

(43) White, F. M. *Fluid Mechanics*; McGrawHill: New York: 1994.

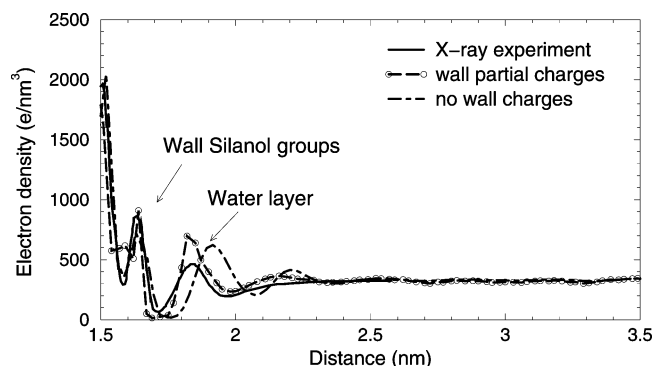(44) Karniadakis, G.; Beskok, A.; Aluru, N. R. *Microflows and Nanoflows*; Springer: New York, 2005.

Figure 2. Electron density plots at the surface of the 4.1 nm channel with partial charges compared to X-ray reflectivity data for water at a 1010 quartz surface. The experimental data is from ref 38.

coefficient and the ionic mobility, respectively, of species i extracted from MD simulations, c_i is the concentration of the ith species, F is Faraday's constant, $\mathbf{u}$ is the velocity of the bulk flow, μ is the viscosity of water, and p is the pressure in the system. The PNP and the Stokes equations are solved iteratively until a self-consistent solution is obtained. The net current per depth, y, through the channel is then given by $I = I^x = F\Sigma_{i=1}^{N} z_i \int \Gamma_i^x \, dz$, where I^x is the x component of the current, N is the total number of ionic species, and Γ_i^x is the x component of the flux, Γ_i. Since the ionic mobilities from MD simulations are available only at discrete wall normal distances from the binning approach, linear interpolation was used to obtain mobilities for continuum calculations.

Two sets of geometries were used. In the first, the same channel dimensions as the MD simulations were used to compare conductances obtained from MD with conductances obtained from PNP and Stokes equations. After verifying that continuum and MD conductances matched, continuum calculations were performed for channels of length 5 μm and with widths of 1.1, 2.1, 2.75, and 4.1 nm. These channels were attached to baths of size 1 μm × 1 μm at both the ends (Figure 1e). A 2D system in the x−z direction was used. Bias voltages ranging from −3 to 3 V were applied at one end. Bulk transport properties computed from the center of the 4.1 nm channel were used in the baths.

V. Results and Discussion

A. Interfacial Electron Density. First, MD simulations were performed with water alone in the channel. Figure 2 compares the electron density calculations for water at the interfacial region of the 4.1 nm channel with that from recent high-resolution X-ray reflectivity studies of liquid water at room temperature over the molecularly flat, annealed 1010 quartz surface.[38] Electron density in MD is computed by a binning method with the density involving contributions from electrons belonging to all the atoms in a particular bin. Our calculations show that there is one layer of water absorbed near the surface which is fully consistent with the X-ray data within the experimental error bar of 1 Å distance indicated in ref 38. MD studies of interfacial structure for water near a hydroxylated Rutile surface also shows only a single layer of associated water layer near a neutral hydroxylated surface.[45] We note in Figure 2 that the location of the first water peak is farther away from the wall for simulations without partial charges, implying that accurate partial charges are necessary to capture the interfacial structure correctly. We did some test simulations with larger magnitude of charges on the silanol oxygens and
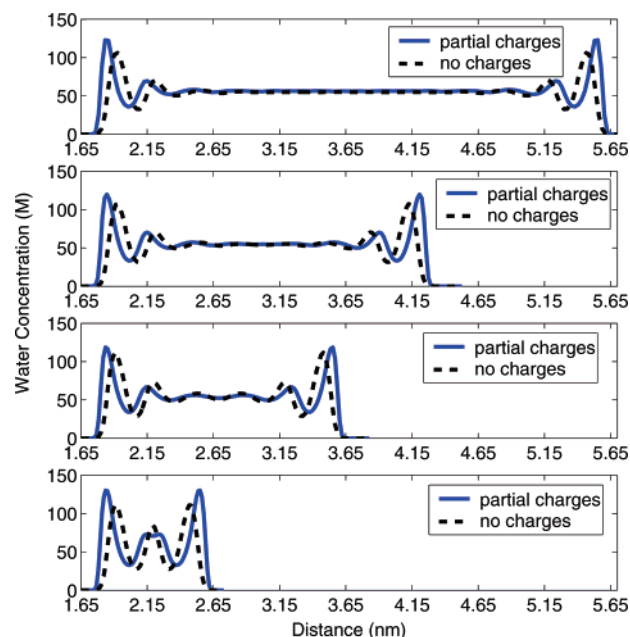
(45) Predota, M.; Bandura, A. V.; Cummings, P. T.; Kubicki, J. D.; Wesolowski, D. J.; Chialvo, A. A.; Machesky, M. L. *J. Phys. Chem. B* **2004**, *108*, 12049.


Figure 3. Water concentration profiles for uncharged and partially charged channels in 4.1 (top), 2.75 (second from top), 2.1 (second from bottom), and 1.1 nm (bottom) channel widths.

bulk silicon as used in other force fields[35] and observed that an additional peak of water was formed between the water peak in Figure 2 and the silanol groups because larger partial charges cause a stronger electrostatic interaction with the surface while experimental observations and present simulations suggest otherwise.

B. Water Structure. To study the effect of the wall partial charges on the interfacial behavior of aqueous solutions in the channels, MD simulations were performed with four different channel widths. Figure 3 shows the water concentration profiles with and without partial charges for 1.1, 2.1, 2.75, and 4.1 nm channels. Concentration variation in the axial x direction was observed to be periodic. In the wall normal z direction, the well-known layering effects were observed. For channels wider than 2.1 nm, the wall normal profile of water shows one distinct peak and two other smaller peaks before reaching the bulk concentration profile. The interfacial water structure remains the same for different widths. Regardless of the channel width, the first peak is located at a distance of 0.2 nm from the wall (which is located at $z = 1.65$ nm) for channels with partial charges and 0.26 nm for channels without any wall charges. The partial charges seem to pull the first peak closer to the wall by a distance of 0.6 Å. To obtain information on the distribution of the water molecules in the x−y plane, relative to the structured surface, we calculated three-dimensional density profiles of water molecules using narrow bins of widths of 0.2 Å in the channel. From this three-dimensional density map, the lateral x−y density profiles in a select layer above the surface are obtained by integrating along the wall normal z direction. In Figure 4, we plot the lateral density profiles of water molecules in the first layer of water for $z < 2.0$ nm. The contour plots show a high degree of water ordering both for charged and uncharged channels in the first layer of the water. The water molecule coverage on the surface corresponds to the crystallographically dictated coverage associated with the surface sites. Though the ordering decreases considerably after the first water layer, lateral x−y ordering is present till about 1 nm ($3\sigma_{O-O}$) into the channel from the wall. The ordered water structure in a rutile−water interface also extends to about $3\sigma_{O-O}$ from the surface till it slowly attains bulk characteristics.[45]
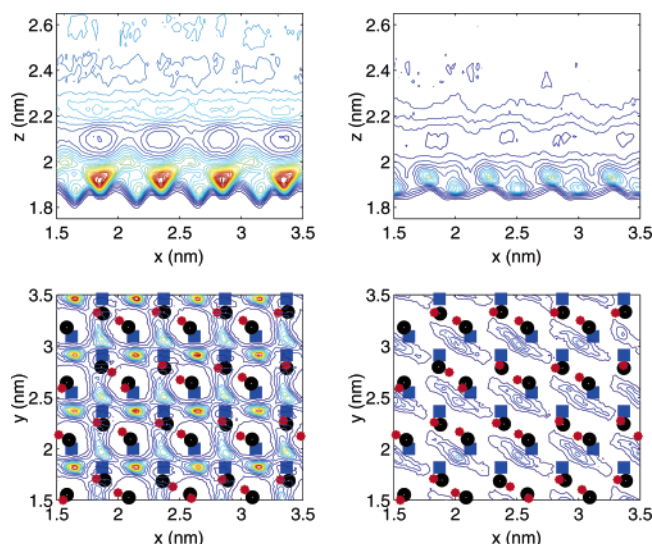
Figure 4. Density contours in the *xz* plane: 4.1 nm uncharged (top left) and 4.1 nm partially charged (top right). Surface density contours in the *xy* plane for a distance of *z* < 2 nm: 4.1 nm uncharged (bottom left) and 4.1 nm partially charged (bottom right). Filled squares denote the positions of the surface silicon atoms, filled circles that of the silanol O atoms, and filled stars that of the silanol hydrogen atoms of a single time step during the simulation.
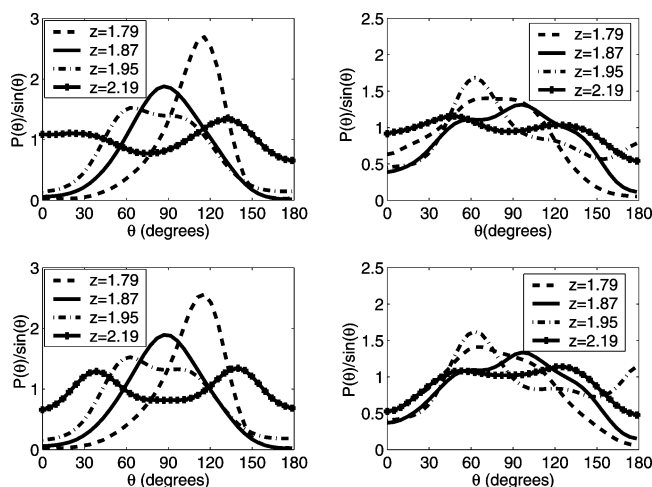

Figure 5. Distribution, $P(\theta)$, of the angle between the normal to the wall and the water dipole vector normalized by the solid angle spanned by the dipole in (top left) 4.1 nm uncharged, (top right) 4.1 nm charged, (bottom left) 1.1 nm uncharged, and (bottom right) 1.1 nm charged channels. The distribution of the dipoles is given at various wall normal distances (*z*) in the legend. Dipole distributions at various sections show that the interfacial water structure remains the same regardless of the channel width.

The water ordering can be further characterized by the dipole orientations of the water molecules in the interfacial region. Figure 5 shows the preferred orientation of water near the surface. For uncharged channels very close to the wall, because of the effect of surface roughness, a preferred ordering of 120° is observed at $z = 1.79$ nm. At a distance of $z = 1.87$ nm, on the side facing the wall of the first layer of water, the angle between the water dipole and the normal to the surface of the channel is 90°, as commonly seen near hydrophobic surfaces. Partial charges enhance the ordering of water. When the channel has partial charges, the water closest to the wall is oriented at an angle of 70−80° to the normal in such a way that some of them form hydrogen bonds with the wall surface and other water molecules are oriented so as to form hydrogen bonds with the water away from the surface. Just beyond the first water peak, at $z = 1.87$
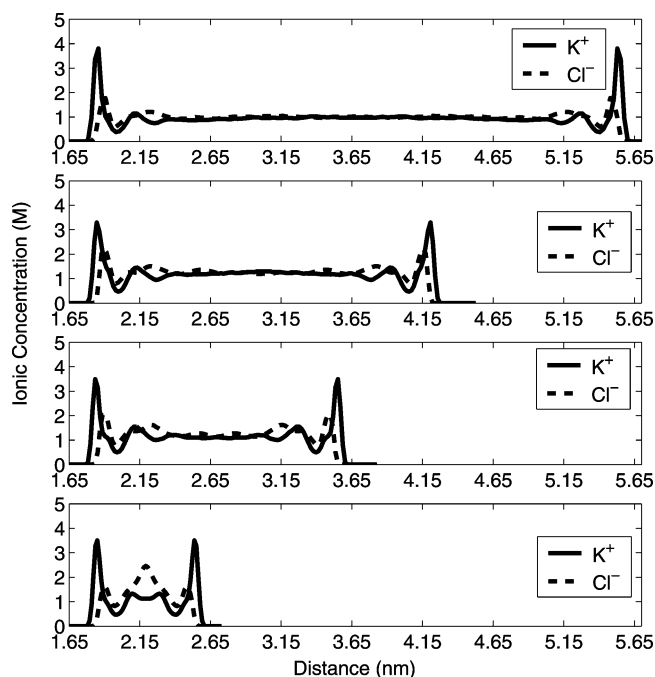

Figure 6. Comparison of K^+ and Cl^- ion concentration profiles for the partially charged slits of four different widths of 4.1 (top), 2.75 (second from top), 2.1 (second from bottom), and 1.1 nm (bottom) channel widths.

nm, the orientation is around 90−100°. At a distance of $z = 1.95$ nm, again an orientation of predominantly 60° is seen which represents water molecules forming hydrogen bonding with the second water layer. Comparing 1.1 and 4.1 nm channels in Figure 5, the water dipole orientation distributions are similar at $z = 1.79$, 1.87, and 1.95 nm showing that the water structure near the interface is similar regardless of the channel width. However, at a distance of $z = 2.19$ nm for both partially charged and uncharged channels, as the water structure approaches bulk region, the dipole orientation distributions in the 1.1 nm channel and the 4.1 nm channel are not quite similar. This is because, in 4.1 nm channel, water orientation at a distance of 2.19 nm is such that they connect with the less-ordered bulk region without any preferred orientations, but in the 1.1 nm channel, $z = 2.19$ nm is the channel center region which still retains the ordered structure with preferred orientations.

C. Ion Concentration Profiles. Figures 6 and 7 show the ionic concentration profiles with and without partial charges, respectively, for various channel widths. When the channel has partial charges, K^+ ion approaches closer to the wall (see Figure 6) compared to Cl^- ions. Even though the concentration difference between the anions and the cations is not as large as seen in charged surfaces,[9] the ratio of the cations to the anions in the first layer is around 1.8−2.1 for different channel widths. The K^+ concentration in the interfacial layer is about 3.6 times larger than that in the bulk. X-ray reflectivity results on the structure of the K^+ and Cl^- ions in the interface region are not easy to obtain because of the small differences in electron density between ions and water.[45]

In the case of an uncharged 1.1 nm channel, we observe that K^+ ions form a peak at the center and the Cl^- ions approach closer to the wall than K^+ ions (see Figure 7). Though not so pronounced, the surface characteristics of larger channels are also the same. Even in 4.1 nm uncharged channels, Cl^- forms a half peak close to the surface followed by alternating peaks of K^+ and Cl^- ions till about 2.8−3 nm beyond which the concentrations of the K^+ and Cl^- ions are the same.
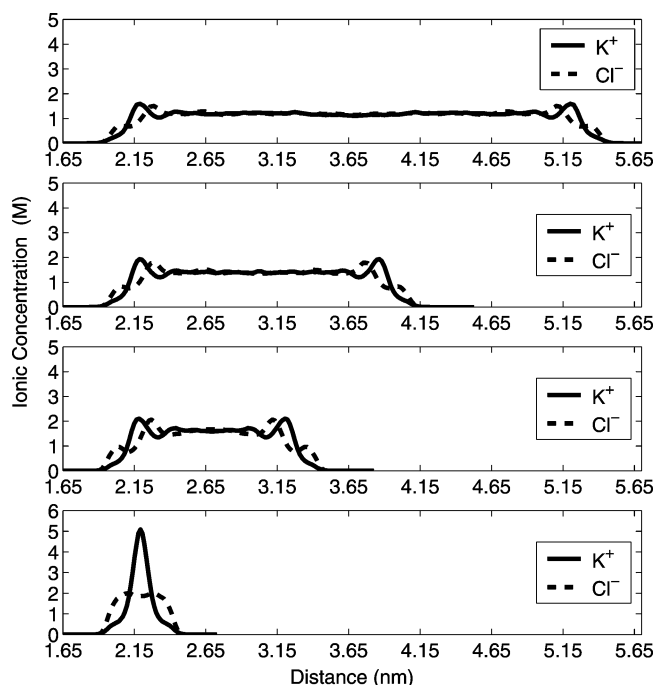
Figure 7. Comparison of K^+ and Cl^- ion concentration profiles for the uncharged slits of four different widths of 4.1 (top), 2.75 (second from top), 2.1 (second from bottom), and 1.1 nm (bottom) channel widths.
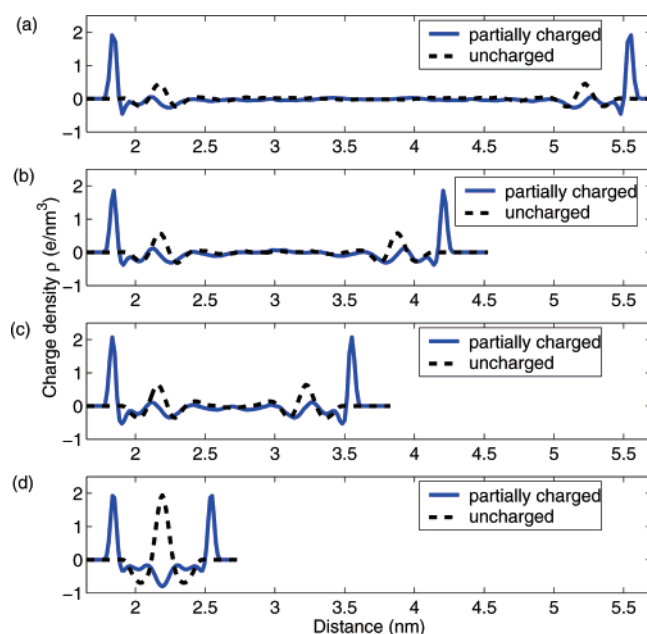

Figure 8. Net ionic charge density across the width of the channel for various channel widths. (a) 4.1 (b) 2.75 (c) 2.1, and (d) 1.1 nm.

One of the most interesting phenomena arising from these concentration distributions is the existence of an electric double layer near the surface when the net surface charge is zero. In the traditional double layer, there is a higher concentration of the counterions than the co-ions near a charged surface. Here, though, the net surface charge is zero; the cations and anions have different propensities to penetrate the surface water layer. This leads to differences in ionic concentration within the interfacial layer which in turn builds a finite charge and a diffuse layer near the interface. Figure 8 shows the net charge density across the channel arising from the varying concentrations of the ions in the channel. For the partially charged channel, there is a net $+\nu$e charge very near the surface due to the K^+ ions, but for $z > 1.88$ nm, the

crossover of the Cl^- concentration causes the charge density to become negative. After some fluctuations, at about 1 nm from the surface, the charge density eventually approaches zero. In the uncharged channels, for $z < 2.09$ nm, the charge density is negative due to the half peak of Cl^-, but for $2.09 < z < 2.24$ nm, the charge density is positive.

The point of zero charge could be considered a special case of low surface charge density. At a low surface charge density of 0.0081 C/m^2, for a co-ion-to-counterion diameter ratio of 1.5, reference hypernetted chain approximation theory has been used to show that excess counterions near the surface causes an overcompensation of the surface charge leading to the formation of two sharply increasing peaks of counter and co-ions near the wall without further oscillations that reach bulk values at 1 nm from the surface.[46] Since we include explicit water molecules in our simulations, the concentration profiles in our simulations are influenced by wall partial charges, wall LJ interactions and by the interaction of the ions with water. Even for a smaller ion size ratio, $\sigma_{Cl-W}/\sigma_{K-W} = 1.3$ (W denotes the wall Si or O atom), than in ref 46, we observe three oscillations of alternating cations and anions before the profiles reach bulk values at 1 nm from the wall.

In the following section, using the potential of mean force (PMF), we examine the various interactions that determine the ionic concentration profiles near the interface.

D. Potential of Mean Force. The ion concentration profiles for uncharged channels have oscillations that lead to alternating double layers stacked next to each other. In the case of uncharged channels, even though σ_{Cl-W} is greater than that of σ_{K-W}, we note that Cl^- approaches closer to the wall than K^+, forming a half peak which precedes alternating peaks of K^+ and Cl^-. In the case of partially charged channels, one might guess that K^+ forms the first peak near the wall rather than Cl^- because the net charge of the silanol OH group is negative. However, in the wall silanol OH group, hydrogen, with a charge of $+0.44$, is closer to the electrolyte than oxygen, which has a larger magnitude of negative charge of -0.77. To ascertain how the local electrostatic interactions from the wall affect the ion concentration profiles, we need to examine the forces acting on the ions.

When an ion, i, moves along the wall normal direction from z_o to z, the work done, $W_i(z) - W_i(z_o)$, is computed by integrating the mean force $\langle F_i(z) \rangle$ acting on the ion along the wall normal direction contributed by all other atoms in the system averaged over all the configurations,[47] i.e.,

$$W_i(z) - W_i(z_o) = \int_{z_o}^{z} \langle F_i(z') \rangle \, dz' \qquad (6)$$

where z_o is the reference position. For the 4.1 nm channel, the reference position is the center of the channel where the PMF is defined to be zero. We obtained the mean force distribution by sampling the force experienced by the ions in bins at different wall normal distances for both partially charged and uncharged 4.1 nm channels.

Figure 9 shows the PMF acting on the ions for the 4.1 nm uncharged channel. Figure 9a shows the concentrations of water and ions as a function of the wall normal z distance, and Figure 9b shows the PMF for K^+ and Cl^- ions. The PMF is related to the Boltzmann distribution, whereby when the concentration of ions is maximum, the PMF is minimum. The peaks in the concentration profiles correspond to valleys in the PMF. To obtain a better understanding of the concentration profiles and the location of the peaks of K^+ and Cl^- ions, we decompose the

(46) Greberg, H.; Kjellander, R. *J. Chem. Phys.* **1998**, *108*, 2940.
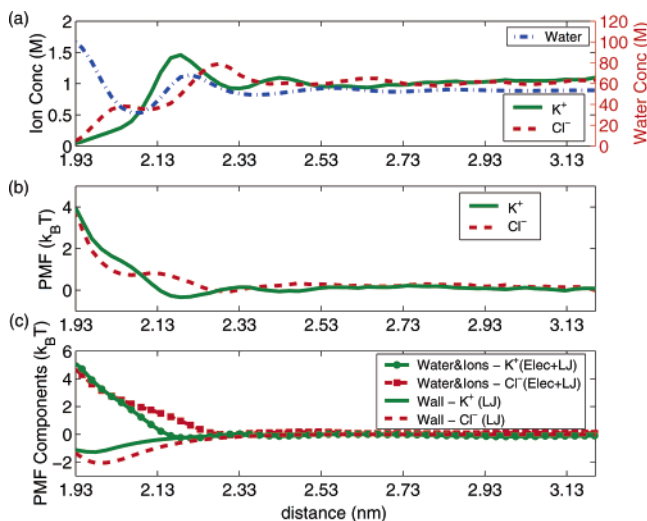(47) Kjellander, R.; Greberg, H. *J. Electroanal. Chem.* **1998**, *450*, 233.

Figure 9. PMF showing the effect of non electrostatic forces from the wall on the ionic concentration profile for an uncharged channel. (Top) Concentration profiles for water, K^+, and Cl^- ions. (Second from top) PMF of the ions (Bottom) Split up of the PMF into the contribution of the wall (Lennard−Jones) and that from water and ions including both electrostatic and LJ components. The half peak of Cl^- in the range 1.93 nm $< z <$ 2.09 nm is caused because the wall−Cl^- LJ interaction is more favorable than wall−K^+ LJ interaction in that range.

PMF of the ions into its different components. Figure 9c separates the contribution from the wall and rest of the atoms (water and ions). The contribution to the PMF from the wall is due to the wall−ion LJ interactions. Since the LJ parameter $\sigma_{K-Si} < \sigma_{Cl-Si}$ and $\sigma_{K-O} < \sigma_{Cl-O}$, K^+ ions would normally be expected to approach closer to the wall than Cl^- ions. However, for 1.93 < z < 1.96 nm, where wall−K^+ LJ interaction has its minimum, the water−ion interactions (Figure 9c) are large enough to prevent K^+ ions from crossing over the water peak at z = 1.93 (Figure 9a) and approaching close to the wall. For 1.93 < z < 2.09 nm, the LJ contribution for Cl^- is more favorable (Figure 9c) and this causes the PMF for Cl^- in Figure 9b to be lower than that of K^+ for 1.93 < z < 2.09 nm. The first semi peak of Cl^- (Figure 9a) for 1.93 < z < 2.09 nm is therefore due to the wall−Cl^- LJ interactions. Figure 9c also shows that the interactions from water and ions (LJ + electrostatic) on the ions is more favorable for K^+ than Cl^- for 2.09 < z < 2.25 nm causing the first K^+ peak.

Figure 10 shows the concentration variation of water and ions and the PMF acting on the ions for the partially charged 4.1 nm channel. The PMF minimum corresponds to the peaks in the concentration profiles. Figure 10c shows the contributions to the PMF from the wall including both electrostatic and nonelectrostatic interactions on the ions. Also shown is the contribution from the wall LJ interactions alone. At z = 1.8 nm, just into the first K^+ peak, the sum of electrostatic, as well as nonelectrostatic, interactions from the wall is about −16 k_BT for K^+ ions and −10 k_BT for Cl^- ions. The nonelectrostatic contribution from the wall is 21 k_BT for K^+ ions and 42 k_BT for Cl^- ions. Subtracting the nonelectrostatic contributions from the sum, the electrostatic wall−ion interactions from the wall at z = 1.8 nm for K^+ ions is about −37 k_BT for K^+ and that for Cl^- is about −52 k_BT. Very close to the wall, due to the presence of positively charged hydrogen atoms from the silanol groups, electrostatic interactions from the wall are more favorable for Cl^- ions. However, at the same time, the wall−ion LJ interactions are more repulsive for Cl^- than K^+ (Figure 10c) such that the combined interaction is more favorable for K^+.
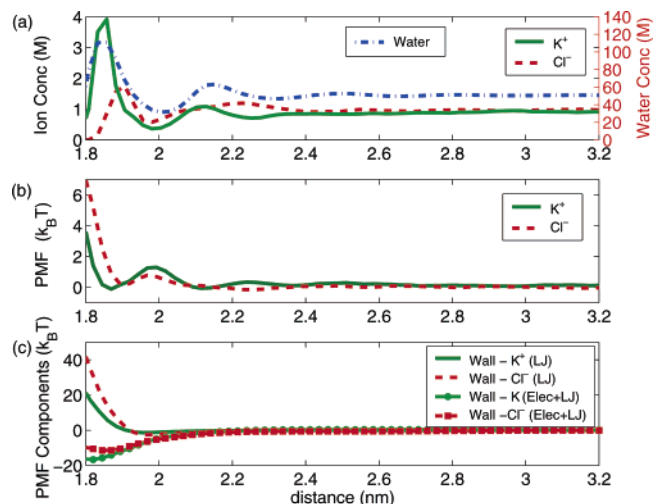

Figure 10. PMF showing the effect of wall−ion interactions on the ionic concentration profile for a channel with wall partial charges but net zero charge.(Top) Concentration profiles for water, K^+, and Cl^- ions. (Second from top) Total PMF of the ions. (Bottom) The total contributions from the wall on the PMF of ions (electrostatic + LJ) and the contribution from LJ interactions alone. At z = 1.84, at the first K^+ peak, the total wall−ion interactions is favorable for K^+.
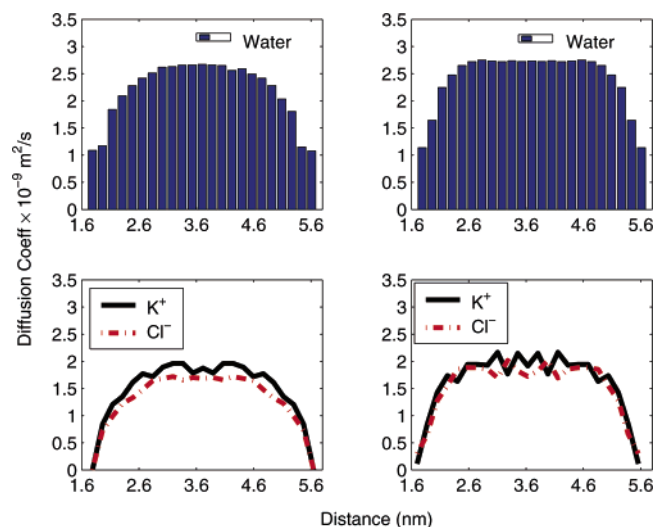

Figure 11. Diffusion coefficient of water and ions in uncharged and charged 4.1 nm channels. Uncharged channels are on the left column, and the partially charged channels on the right. The top row has the diffusion coefficients of water and the bottom row has that of ions.

E. Water and Ion Diffusivity. To ascertain whether there are any immobile layers of ions and water near the surface as frequently suggested in the literature,[7] we calculated the mean square displacement of water and ions and obtained the diffusion coefficients. The diffusion coefficient is normally calculated as $D = \lim_{t\to\infty} 1/6 \langle (r_i(t) - r_i(0))^2 \rangle$. To understand the diffusivity along the surface in the axial direction, we obtain $D_x = \lim_{t\to\infty} 1/2 \langle (x_i(t) - x_i(0))^2 \rangle$ parallel to the surface. To calculate the variation of the axial diffusion coefficient along the width of the channel, we divided the channel into several bins. The linear part of the MSD plot was used to compute the diffusion coefficient. Figures 11 and 12 show the diffusion coefficients of water and ions for 4.1 and 1.1 nm channels, respectively. In the case of the 4.1 nm channel, both for partially charged and uncharged cases, the diffusion coefficient of water is around 38% of the bulk value (2.7 × 10^{-9} m²/s for SPC/E water at 300 K[48]) very close
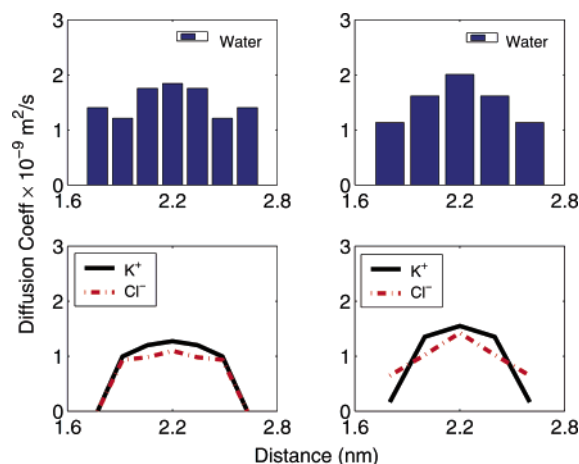
Figure 12. Diffusion coefficient of water and ions in uncharged and charged 1.1 nm channels. The top row has the diffusion coefficients of water, and the bottom row has that of ions. Uncharged channels are on the left column, and the partially charged channels on the right.

to the surface in the first water layer. However, within about 1.5 nm from the surface, the bulk value is reached. The experimental value of diffusivity of water in 1 M KCl is $2.63 \pm 0.13 \times 10^{-9}$ m²/s[49] at 298 K. The agreement between SPC/E model and experimental value for diffusivity is better than majority of the existing water models. When water is severely confined in a 1.1 nm channel, the reduction in the diffusivity is more drastic, with no bulk values being attained. The ionic diffusion coefficients also show a decrease in diffusivity compared to the bulk. In the bulk, the values are close to the experimental bulk diffusion coefficients of K^+ and Cl^- at 1 M. The experimental values of bulk diffusion coefficients of ions in 1 M KCl at 298 K are 1.865 $\times 10^{-9}$ and 1.931×10^{-9} m²/s for K^+ and Cl^-, respectively.[49] However, in the interfacial layer, the diffusion coefficients reduce primarily because of the increased water ordering near the surface which retards the free movement of the ions.

In our simulations, even though the interfacial diffusion coefficient of water is significantly less than that in the bulk, it is not approaching zero. This suggests that water in the first layer is not completely immobile as in solid ice. Though there is a well-ordered two-dimensional hexagonal arrangement of water molecules near the surface, the hydration layer is dynamic and not static. Ab initio MD simulations have been used to show adsorption of water on a fully hydroxylated β cristobalite silica surface.[50] Very close to the surface, a well-ordered two-dimensional ice structure with polygonal patterns of hydrogen-bonding network is observed. In our simulations, we do observe hexagonal arrangement of water molecules very close to the surface which in contour form is shown in Figure 4, but we do not see the water molecules immobilized completely. This could be because in the ab initio calculations, there is only a single layer of water molecules being simulated above the silica surface with the water molecules interacting only with the silica surface. Because we are able to simulate a much larger number of molecules in MD simulations, interactions of the first layer of water with layers in the channel center are also considered. Long-range electrostatic interactions of the water in the channel with the surface water layer reduces the probability of water being immobilized on the surface. Our results are more in line with the
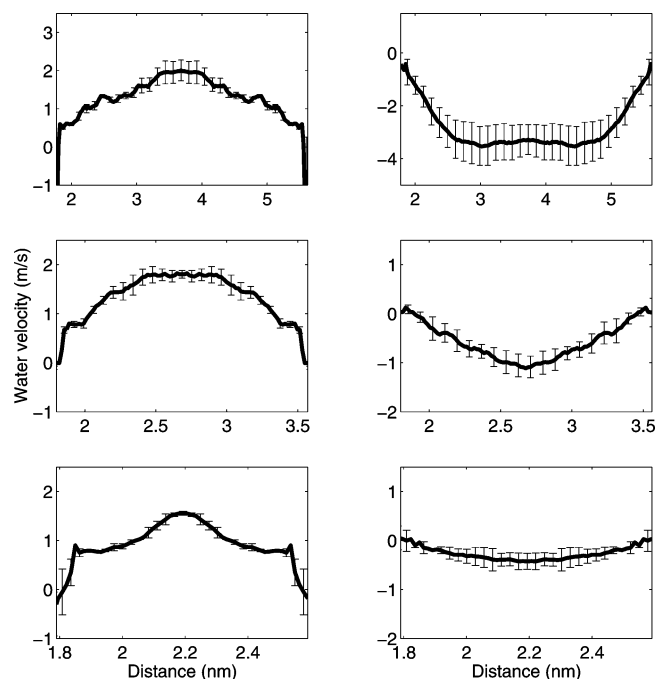

Figure 13. Electro-osmotic velocity profiles across the width of the 4.1 (top), 2.1 (middle), and 1.1 nm (bottom) channel widths under an external electric field of 0.35 V/nm. Uncharged channels are on the left column, and the partially charged channels are on the right column.

recent MD simulations of confined water in mica[51] where persistent fluidity of surface bound hydration layers of water is observed even under extreme confinement.

F. Electro-osmotic Flow. Electro-osmotic flow generated due to the electric double layer (EDL) near charged surfaces has been extensively investigated over the years,[8,52] and recent experiments on silica nanochannels show that the transport in nanochannels is dominated by the effective surface charge.[4,5] Experimental observations from Chaiyasut et al.[53] show that naturally induced charges have a significant role in electro-osmosis in silanol-terminated channels and that even when a large negative surface charge is present, about 10% of the electro-osmotic flow is from naturally induced charges. Measurements on ζ potential in hydrophobic graphite surfaces show the existence of a double layer due to van der Waals and other hydrophobic surface forces even when there is no induced surface charge present.[54] To quantify the electro-osmotic flow, we apply an external electric field of 0.35 V/nm. Such a field can be considered large, but this is well within the range of dielectric breakdown strength since experiments with quartz surfaces show that the dielectric breakdown occurs around 0.7 V/nm.[55] The oscillations in the ion concentration profiles give rise to electro-osmotic flow even though the solution in the channel is electroneutral (see Figure 13). Electro-osmotic flow is observed when the channels are uncharged or have partial charges but the direction of the flow is different in both cases.

The standard electric double layer description predicts a linear relationship between the electro-osmotic flow velocity and the applied electric field by the Helmholtz−Smoluchowski equation:[8]

(48) Smith, P. E.; van Gunsteren, W. F. *Chem. Phys. Lett.* **1993**, *215*, 315.
(49) Mills, R.; Lobo, V. M. M. *Self-Diffusion in Electrolyte Solutions*; Elsevier: Amsterdam, 1989.
(50) Yang, J.; Meng, S.; Xu, L.; Wang, E. G. *Phys. Rev. B* **2005**, *71*, 035413.
(51) Leng, Y. S.; Cummings, P. T. *Phys. Rev. Lett.* **2005**, *94*, 026101.
(52) Hunter, R. J. *Zeta Potential in Colloid Science*; Academic: New York, 1981.
(53) Chaiyasut, C.; Takatsu, Y.; Kitagawa, S.; Tsuda, T. *Electrophoresis* **2001**, *22*, 1267.
(54) Fa, K. Q.; Paruchuri, V. K.; Brown, S. C.; Moudgil, B. M.; Miller, J. D. *Phys. Chem. Chem. Phys.* **2005**, *7*, 678.
(55) von Hippel, A.; Maurer, R. J. *Phys. Rev.* **1941**, *59*, 820.

$$U = -\frac{\epsilon\zeta}{\mu}E \tag{7}$$

where U is the mean electro-osmotic velocity, ϵ is the dielectric permittivity, ζ is the zeta potential, μ is the viscosity, and E is the applied electric field. To compare the effect of the pseudo double layer in partially charged or uncharged channels with literature, in line with experimental procedures, we compute an *apparent ζ potential*[56] in the 4.1 nm channel where bulk values have been attained in the center. Using the bulk values of viscosity and permittivity for water and an applied electric field of 0.35 V/nm, we obtain an apparent ζ potential of -8 mV for an electro-osmotic flow of 2 m/s in the uncharged channel and 12 mV for a velocity of 3 m/s in a partially charged channel. For alumina surfaces with zero surface charge, a ζ potential of 8 mV has been observed at 1 M KCl concentration.[14]

Since the local charge density is nonzero in the interfacial region (Figure 8), locally there is a nonzero driving force arising from local charge density, although the net driving force is zero. The net flow profile is due to the combined action of the local driving forces and the water ordering. The velocity profile in the center is more or less flat within the error bars. In the partially charged case, the driving force is positive for $z < 1.88$ nm due to an increased cation concentration and negative for $z > 1.88$. However, the high degree of water ordering and the decreased diffusion coefficient for $z < 1.88$ nm (Figure 4) make the water less mobile in this region such that the net flow is driven by the local negative charge density in the region $z > 1.88$ such that the net flow is in the negative direction. In the case of the uncharged channel, the local charge density alternates between positive and negative values and the resultant flow is in the postive direction. Although the magnitude of the local charge densities are not as large as in the partially charged case, velocity is enhanced due to the sharp jump in the velocity profile near the surface. The fact that the water density in the jump region is extremely low and that the water dipoles there orient parallel to the surface with hydrogen bonds to each other but not toward the wall is conducive to shearing under the action of a driving force. However, when partial charges are present, the water density in that region is higher and the hydrogen-bonded interactions between the water and the wall do not allow a jump in the velocity.

G. Ionic Mobility. To obtain the ion mobilities, ion distribution in the channel was computed by using the binning method, and the ion velocity was computed by tracking the positions of the ions. Because the electro-osmotic component is about one-fifth of the total velocity and is not negligible, we subtract the electroosmotic velocity from the velocity of ions in each bin before dividing by the electric field strength to obtain the mobility. Figure 14 shows the variation of ion mobility profiles for partially charged and uncharged channels. Near the surface, the mobilities are low, but they gradually increase toward the channel center. When there are no partial charges, the mobility reaches the bulk value closer to the wall than with partial charges.

To compare the mobilities in the channel center of a 4.1 nm uncharged channel with that in the literature, the bulk mobilities are represented by equivalent conductivities defined as[57]

$$\Lambda = -\frac{\sigma}{c} \tag{8}$$

(56) Joly, L.; Ybert, C.; Trizac, E.; Bocquet, L. *Phys. Rev. Lett.* **2004**, *93*, 257805.
(57) Shedlovsky, T. *J. Am. Chem. Soc.* **1932**, *1411*, 125502.
(58) Snyder, K. A.; Feng, X.; Keen, B. D.; Mason, T. O. *Cement Concrete Res.* **2003**, *33*, 793.
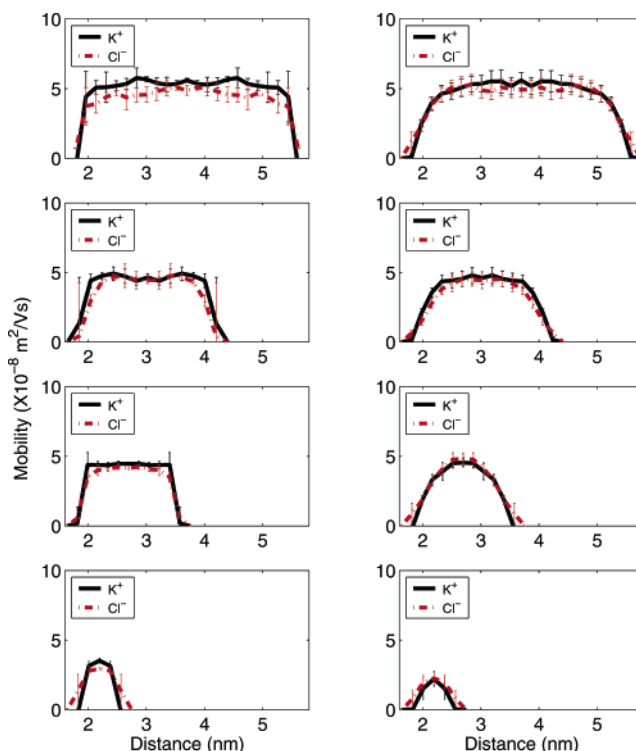

Figure 14. Ion mobilities for uncharged and charged channels. 4.1 (top), 2.75 (second from top), 2.1 (second from bottom), and 1.1 nm (bottom) channel widths. Uncharged channels are on the left column, and the partially charged channels on the right column. The error bars denote the uncertainty in the computed values of the mobility.

Table 5. Ionic Conductivity in the Center of the Uncharged 4.1 nm Wide Channel

equivalent conductivity (cm^2S/mol)	this work	experiment 1[58]	experiment 2[57]
1 M	102.49 ± 1.94	103	112

where σ is the conductivity defined as $cF\mu$, where c is the ionic concentration, F is the Faraday constant, and μ is the mobility of the ions. The equivalent conductivity of the center portion of the 4.1 nm uncharged channel is compared with experimental equivalent conductivities at 1 M concentration in Table 5 showing reasonable agreement.

H. $I-V$ Curves in a Channel-Bath System. Using transport properties from atomistic simulations, we obtained the (current-(I) vs voltage(V)) $I-V$ curves in channel-bath systems using continuum theory. First, to ascertain whether the continuum models can adequately reproduce conductivities from MD simulations, we computed ionic conductances from continuum theory for the same channel dimensions as used in MD simulations with the same external electric field. The only parameter used from MD was the mobilities at discrete bins. The conductances from MD calculations are computed as follows

$$C = -\frac{\mu cFA}{L} \tag{9}$$

where A and L are the area of cross section and length of the channel, respectively. The mobility, μ, is computed by dividing the mean velocities of all the ions in the channel with the electric field. For continuum calculations, mobilities computed at discrete z locations were used. The comparison is shown in Table 6. The MD and PNP calculations show very similar conductances.

Once the continuum model has been shown to produce the same conductances as MD, we performed continuum calculations
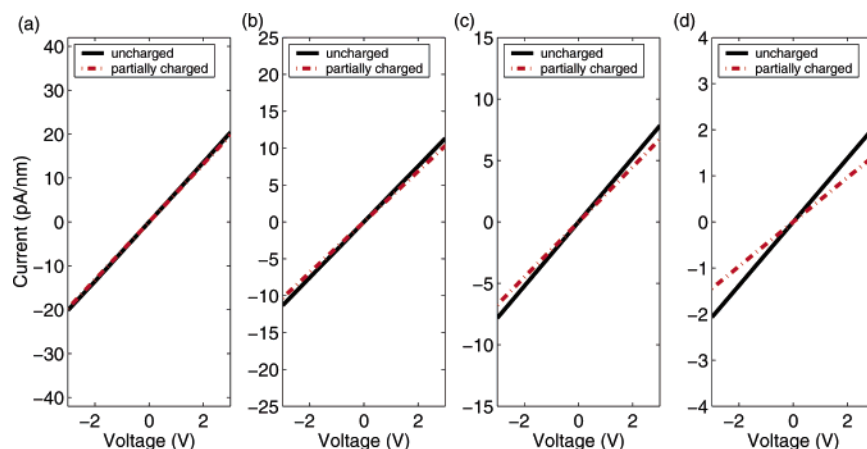
Figure 15. $I-V$ curves for various channel widths: (a) 4.1 (b) 2.75 (c) 2.1, and (d) 1.1 nm.

Table 6. Ionic Conductance: Comparison with MD and PNP

conductance ($\times 10^{-7}S$)	4.1 nm	2.75 nm	2.1 nm	1.1 nm
MD (no partial charges)	0.3694	0.2092	0.1402	0.0437
PNP (no partial charges)	0.3612	0.2027	0.1396	0.0380
MD (partial charges)	0.3564	0.1875	0.1275	0.0243
PNP (partial charges)	0.3589	0.1873	0.1204	0.0242

on channel-bath systems. Channels of the same widths as in MD simulations but with lengths of 5 μm were used to connect baths of micrometer dimensions (see Figure 1e). Figure 15 shows the macroscopic $I-V$ curves from continuum theory for different channel widths. At strengths of 1 M KCl, for channel widths of the order of $1-2$ nm, the quantum partial charges reduce the magnitude of the current significantly, but when the channel is 4.1 nm in width, the effect of the quantum partial charges is not so pronounced. As the channel width increases, the contribution of the surface current is smaller, so at 4.1 nm channel width, the net conductivity of partially charged and uncharged channels is the same.

VI. Conclusions

In summary, we demonstrate a hierarchical multiscale methodology to solve ion transport in nanoscale channels and show that the partial charges from quantum calculations significantly alter transport properties of electrolytes in confined geometries. The computed quantum partial charges are in good agreement with experiments, and MD simulations with these charges match well with X-ray reflectivity measurements. MD simulations with partial charges show significant variation in the water ordering and structure in the nanochannel. The quantum contributions of the wall−electrolyte interactions are substantial up to a distance of about 1 nm from the surface and alter the bulk transport in channel widths of the order of $1-2$ nm. From the water structure and ionic concentration profiles, it can be concluded that, for both partially charged and uncharged channels, an electric double layer is established since the distance of closest approach for cations and anions is not the same. Since water molecules have dipole moments associated with them, they assume a preferential orientation at the surface. The presence of the ions and the wall partial charges change the interfacial orientation of water from that of water near an uncharged surface affecting the properties of the electric double layer near the interface. Contrary to expectations from continuum theory, electro-osmotic flow is observed in charged and uncharged channels, and flow reversal is observed in partially charged channels. Using mobility values from MD in continuum theory, we computed macroscopic $I-V$ curves in channel-bath systems of micrometer dimensions with the same channel width as in MD. The quantum partial charges affect the $I-V$ curves for channel widths <4.1 nm.

LA0610147